MODELING OF STRAIN PENETRATION EFFECTS IN FIBER-BASED ANALYSIS OF REINFORCED CONCRETE STRUCTURES

Jian Zhao and Sri Sritharan

Biography: ACI member **Jian Zhao** is an assistant professor in the Department of Civil Engineering and Mechanics at the University of Wisconsin at Milwaukee, WI. He received his PhD from the University of Minnesota, Minneapolis, MN and served as a post-doctoral researcher at Iowa State University, Ames, IA. His research interests include behavior of reinforced concrete structures and earthquake engineering.

ACI member **Sri Sritharan** is an associate professor in the Department of Civil, Construction and Environmental Engineering at Iowa State University. He received his PhD from the University of California at San Diego, CA. He is the secretary of ACI Committee 341 (Earthquake-Resistant Concrete Bridges) and an associate member of ACI Committee 445 (Shear and Torsion). His research interests include seismic design of concrete structures and earthquake engineering.

ABSTRACT

In flexural concrete members, strain penetration occurs along longitudinal reinforcing bars that are fully anchored into connecting concrete members, causing bar slips along a partial anchoring length and thus end rotations to the flexural members at the connection intersections. Ignoring the strain penetration in linear and nonlinear analyses of concrete structures will underestimate the deflections and member elongation, and overestimate the stiffness, hysteretic energy dissipation capacities, strains and section curvature. Focusing on the member end rotation due to strain penetration along reinforcing bars fully anchored in footings and bridge joints, this paper

introduces a hysteretic model for the reinforcing bar stress vs. slip response that can be integrated into fiber-based analysis of concrete structures using a zero-length section element. The ability of the proposed hysteretic model to capture the strain penetration effects is demonstrated by simulating the measured global and local responses of two concrete columns and a bridge tee-joint system. Unless the strain penetration effects are satisfactorily modeled, it is shown that the analysis of concrete structures will appreciably underestimate the local response parameters that are used to quantify structural damage.

Keywords: reinforced concrete; seismic analysis; strain penetration; fiber analysis; bond slip; column; wall; bridge bent; OpenSees.

INTRODUCTION

There is a growing demand for developing reliable numerical simulation tools that can assist with improving safety of concrete structures under extreme lateral loads, as well as advancing seismic design of structures by addressing multiple performance limits. For reinforced concrete structures subjected to moderate to large earthquakes, capturing the structural response and associated damage require accurate modeling of localized inelastic deformations occurring at the member end regions as identified by shaded areas 1 and 2 in Fig. 1. These member end deformations consist of two components: 1) the flexural deformation that causes inelastic strains in the longitudinal bars and concrete, and 2) the member end rotation, as indicated by arrows in Fig. 1, due to reinforcement slip. This slip, which is characteristically different from the slip that occurs to the entire bar embedment length due to poor anchorage condition,[1] results from strain penetration along a portion of the fully anchored bars into the adjoining concrete members (e.g., footings and joints) during the elastic and inelastic response of a structure. As demonstrated by Sritharan et al.[1], ignoring the strain penetration component may appear to produce satisfactory force-displacement response of the structural system by overestimating the flexural action for a given lateral load. However, this approach will appreciably overestimate the rebar and concrete strains and section curvatures in the critical inelastic regions of the member, thereby overestimate the structural damage. These strain increases do not necessarily lead to a significant increase in the moment resistance at the section level because the increase in the resultant force magnitudes will be compensated by reduction in the moment arms, thereby producing satisfactory force-displacement response for the member. Since the objective of the finite element analyses is to produce satisfactory global and local responses, an accurate representation of the strain penetration effects is critical when developing finite element models of concrete structures.

In beam-column joints of building frames, plastic hinges are designed to form at the beam ends (see shaded area 2 in Fig. 1), causing the beam longitudinal bars to experience slip due to strain penetration that occurs along the bars into the joint. Furthermore, the beam bars embedded in the interior joints of a frame structure responding to earthquake loads will be subjected simultaneously to tension at one end and compression at the other end. This condition, combined with the effects of load reversals, will progressively damage bond along the entire length of the beam bar within the joint, essentially causing slippage of the entire bar within the joint. Hence, the bond-slip of beam bars within the joint is expected to be relatively more sensitive to the concrete strength, anchorage length, and joint force transfer mechanism compared to the column/wall longitudinal bars anchored in footings and bridge joints.

Unlike the beam bars anchored into the interior building joints, the column and wall longitudinal bars extended into footings and bridge joints are typically designed with generous anchorage length (shaded area 1 in Fig. 1). Furthermore, the bars anchored into footings are often detailed with 90° hooks at the ends to improve constructability. In these cases, the embedded longitudinal bars that are loaded only at one end experience slip along a portion of the anchorage length and utilize end bearing to transfer forces when they are subjected to compression.[2] Hence, the monotonic and cyclic behavior of anchored bars (e.g., bar stress vs. slip responses) at the intersection between a flexural member and a footing/bridge joint is expected to be different from that occurring at the building joint interfaces. For these reasons, the hysteretic bar stress vs. slip response of these bars anchored in footings and bridge joints will be relatively more stable and dependable. This hypothesis was evident in the cyclic load tests documented by Lin[3] on a few reinforcing bars that were fully anchored in concrete with straight and hooked ends.

RESEARCH SIGNIFICANCE

A significant effort has been invested to model the bond slip of beam bars anchored into building joints while studies on the strain penetration effects of longitudinal bars into footings and bridge joints are very scarce. Recognizing that the member end rotation at the footing and bridge joint interfaces can be reliably simulated using a zero-length section element, this paper proposes constitutive models for the bar slip due to strain penetration. Using two cantilever columns and a bridge t-joint system, it is shown that fiber-based analyses incorporating zero-length section elements with the proposed constitutive models can accurately capture both the global and local responses of concrete structures.

BACKGROUND

Strain penetration that represents gradual transferring of longitudinal bar forces to the surrounding concrete in the connecting member is described in Fig. 2. The loaded end of the anchored bar exhibits slip at the connection interface resulting from the accumulative strain difference between the bar and concrete within the connecting member. As a result, a crack forms at the connection interface and an end rotation occurs to the flexural member. Experimental studies have generally reported that this end rotation contributes up to 35 percent to the lateral deformation of flexural members.[4-6] The strain penetration and the associated end rotation also greatly influence the localized strains and curvature in the critical regions, and stiffness of the flexural member. Ignoring the strain penetration also affects the energy dissipation capacity of the members, but to a lesser extent. Presented below is a brief discussion on the available methods for modeling the bond-slip rotation, followed by details of the analytical method used in this study.

Previous Analytical Methods

Researchers have made significant efforts to model the bond slip of bars anchored into building joints. These efforts range from establishing the local bond stress vs. slip relation[7-11] to quantifying the bond slip effects at the member level through different analytical means.[12-17] General 3-D solid finite element models incorporating gap/interface elements have been used to capture the interaction between anchored longitudinal steel bars and surrounding concrete.[12-15] In these studies, local bond stress vs. slip models such as that developed by Eligehausen et al.[7] were used to describe the constitutive relation for the interface elements. While the suitability of modeling concrete as a homogeneous material at a dimension as small as the bar deformation needs further investigation, the required fine mesh of elements makes this analytical approach prohibitively expensive. Hence, such a general finite element analysis cannot be extended for the simulation of structural responses.

To lower the computational cost, special fiber-based, beam-column elements have been formulated that consider the slippage of the reinforcing bars in the state determination at the section level.[17-19] The reinforcement slippage is quantified by analyzing the bar anchorage in concrete between the adjacent integration points of the beam-column element. Although this special element formulation combines the simplicity of the fiber-based concept (that is discussed in the next section) and accuracy of the finite element analysis, modeling of strain penetration effects is still expensive due to the extensive discretization required to satisfactorily capture the behavior of reinforcing bars embedded in concrete. Furthermore, this analysis approach has been shown to adequately predict the force-displacement response of flexural members; however, its ability to predict localized responses (e.g., strains and curvature) has not been demonstrated.

With referenced to the above mentioned approaches, it should be noted that some controversy has arisen. The local bond-slip models utilized in theses approaches (e.g., Eligehausen et al.) were developed using pull-out tests of reinforcing bars with short anchorage length. In these tests, slippage of bars occurred when they were subjected to small strains. Shima et al.[10] and Mayer and Eligehausen[20] have suggested that bond condition of these bars may not be similar to that of fully anchored bars that experience high inelastic strains.

On a macroscopic level, nonlinear rotational springs have been used at the end of beam-column elements to include the member end rotation due to strain penetration effects.[21, 22] The monotonic properties of the rotational springs are typically established using empirical methods, and the modified Takeda model[21] has been used to describe the cyclic behavior of the rotational springs. Despite the simplicity, the strain penetration effects can not be accurately represented using the rotational springs due to their empirical nature.

The spring model concept has been further advanced by introducing super-elements to model the member end rotation in 2-D frame analyses, in which uniaxial springs are used to represent the slippage of the outermost longitudinal bars in the section.[23, 24] The constitutive model (i.e., bar force vs. slip relationship) for the uniaxial springs is established separately by analyzing the anchorage of the extreme bars. In this analysis, the bond stress distributions along the elastic and inelastic portions of the anchored bar are assumed as adopted by Ciampi et al.,[25] from which a multi-linear bar stress distribution along the anchorage length is established. Using a theoretical stress-strain model for the reinforcing steel, the corresponding strain distribution and thus the slip of the bar at the loaded end are determined. The member end rotation is found by dividing the slip determined for the extreme tension reinforcing bar by the distance to the location of the reinforcement from the neutral axis. This distance, which is determined through a section analysis, is usually assumed to be constant and independent of the amount of bar slip. The monotonic curve established for the moment vs. end rotation relation is often simplified as a piecewise linear curve, and multi-linear unloading-reloading rules are specified so that the frame analyses can be performed under cyclic loading.

The deficiencies of the spring model concept are attributed to the following: 1) the assumed bond stress distribution along the bar is not experimentally justified; 2) the bond slip estimated at the loaded end of the bar is strongly influenced by the theoretical stress-strain model used for the reinforcing steel; and 3) end rotations are underestimated at small displacements due to the use of a constant neutral axis depth. In addition, the spring models may not be reliably extended to capture the bond-slip rotation of a generalized flexural member (that has an arbitrary cross-section and is subjected to bi-directional loading).

Fiber-based Analysis

The fiber analysis concept is briefly reviewed prior to introducing its application to model the strain penetration effects in reinforced concrete flexural members. In this concept, the flexural member is represented by unidirectional steel and concrete fibers. Because the steel and concrete fiber responses are specified in the direction of the member length, the fiber analysis can be used to model any flexural member regardless of its cross-sectional shape or the direction of the lateral load.

The fiber analysis typically follows the direct stiffness method, in which solving the equilibrium equation of the overall system yields the nodal displacements.[19, 20] After the element displacements are extracted from the nodal displacements, the element forces are determined and the member stiffness is upgraded, based on which the global stiffness matrix is assembled for the next time step. The stiffness and forces of the fiber-based elements are obtained by numerically integrating the section stiffness and forces corresponding to a section deformation (i.e., axial strain $\bar{\varepsilon}$ and curvature φ).

The section deformation is calculated by interpolating the element end deformations (i.e., displacement and rotation) at the integration points. From the section deformation, the strain in each fiber (ε) is obtained using the plane sections remain plane assumption. (E.g., $\varepsilon = \bar{\varepsilon} + \varphi y$, where y is the distance of the fiber from the centroid of the section.) The fiber stress and stiffness are updated according to the material models, followed by upgrading of the section force resultant and the corresponding stiffness. The neutral axis position of the section at an integration point is determined through an iterative procedure, which balances the force resultants at the section level as well as at the member level.

Although shear-flexure interaction is not integrated in the element formulation and the built-in plane-section assumption may not be appropriate for some members, fiber analysis remains the most economic and accurate means to capture seismic behavior of concrete structures.[19, 20] In addition, if the member end rotation due to bond slip resulting from strain penetration effects can be accurately modeled, fiber analysis has the potential to accurately predict the localized structural responses such as bar strains and section curvature. Using the zero-length section element available in OpenSees (Open System for Earthquake Engineering Simulation),[27] it is shown in this study that the end rotation due to bond slip can be accurately accounted for in fiber-based analysis of concrete structures. This procedure for capturing strain penetration effects can be adopted in other analysis packages with fiber-based formulations.

Zero-Length Section Element

A zero-length section element is a fiber discretization of the cross-section of a structural member as shown in Fig 3. Such an element is generally used for section analyses to calculate the moment–curvature responses. In a section analysis, the concrete and steel fiber strains are calculated for a given curvature using the plain-section assumption. The fiber forces, obtained using the stress-strain relationship of fibers, are integrated across the section to obtain the corresponding moment. To utilize a zero-length section element in OpenSees, a duplicate node is required (i.e., the distance between node *i* and *j* is zero in Fig. 3). In addition, the translational degree-of-freedom of the nodes should be constrained to each other to prevent sliding of the beam-column element at node *j* in Fig. 3 under lateral loads because the shear resistance is not included in the zero-length section. Described below is a method that uses a zero-length section element to capture the member end rotation resulting from the strain penetration effects.

PROPOSED METHOD

A zero-length section element at the end of a beam-column element as shown in Fig. 3 can incorporate the fixed-end rotation caused by strain penetration to the beam-column element. This is because the zero-length section element in OpenSees is assumed to have a unit length such that the element deformation (e.g., rotation) is equal to the section deformation (e.g., curvature). Because of the fiber representation of the section at the member interface, the proposed approach models the bond slip of the longitudinal bars individually during the state determination of the zero-length section element. Hence, this approach is amenable to the fiber analysis concept and allows the strain penetration effects to be captured during flexural analysis of concrete members regardless of the cross-sectional shape and direction of the lateral load. The concept of using a zero-length section element to capture strain penetration effects is equally applicable to beam bars anchored into interior buildings joints. However, such application of the proposed concept requires further research and is beyond the scope of this paper.

The unit length assumption also implies that the material model for the steel fibers in the section element would represent the bar **slip** instead of **strain** for a given bar stress. Focusing on capturing the bond slip due to strain penetration along fully anchored bars into concrete footings and bridge joints, suitable material models for the zero-length section element are as follows.

Material Model for Steel Fibers

For the selected anchorage condition, the material model for the steel fibers in the zero-length section element must accurately represent the bond slip of fully anchored bars loaded only at one end. To minimize the error in the material model for the steel fibers, the previously discussed approaches involving local bond-slip and steel stress-strain models were not preferred to establish the bar stress vs. loaded-end slip relationship. Instead, a generic model based on measured bar stress and loaded end slip from testing of steel reinforcing bars that were anchored in concrete with sufficient embedment length is advocated in this paper.

Monotonic Curve

It is proposed that the monotonic bar stress (σ) vs. loaded-end slip (s) relationship can be described using a straight line for the elastic region and a curvilinear portion for the post-yield region as shown in Fig. 4. The slope of the straight line was taken as K, whereas the curvilinear portion was represented by,

$$\tilde{\sigma} = \frac{\dfrac{\tilde{s}}{\mu - \tilde{s}}}{\left[\left(\dfrac{1}{\mu \cdot b}\right)^{R_e} + \left(\dfrac{\tilde{s}}{\mu - \tilde{s}}\right)^{R_e}\right]^{1/R_e}}, \tag{1}$$

where $\tilde{\sigma} = \dfrac{\sigma - f_y}{f_u - f_y}$ is the normalized bar stress, $\tilde{s} = \dfrac{s - s_y}{s_y}$ is the normalized bar slip, $\mu = \dfrac{s_u - s_y}{s_y}$ is the ductility coefficient, b is the stiffness reduction factor, which represents the ratio of the initial slope of the curvilinear portion at the onset of yielding to the slope in the elastic region (K), f_y and f_u are, respectively, the yield and ultimate strengths of the steel reinforcing bar, and s_y and s_u are the loaded-end slips when bar stresses are f_y and f_u, respectively.

According to Eq. (1), as the bar stress approaches the yield strength, ($\tilde{s}/\mu - \tilde{s}$) becomes zero, the slip approaches the yield slip (s_y), and the slope of the curve approaches the initial slope (bK). Furthermore, as the bar stress approaches the ultimate strength, ($\tilde{s}/\mu - \tilde{s}$) becomes infinity, the slip approaches the ultimate slip (s_u), and the slope of the curve approaches zero. To maintain a zero slope near the ultimate strength of the bar, the value of factor R_e should be slightly greater than one and was taken as 1.01 for the analyses reported in this paper. The remaining parameters that are required to construct the bar stress vs. slip response envelope are s_y, s_u and b.

The pull-out test data available in the literature for deformed steel reinforcing bars were used to establish a suitable value for s_y. Ensuring that the bar had sufficient anchorage during testing, only the pull-out tests that used a bar embedment length equal to or greater than the minimum anchorage length ($l_{a,\mathrm{min}}$) specified by Eq. (2) were selected for this purpose (see Table 1). The minimum anchorage length was determined equating the bar stress to f_y at the loaded end and assuming an average bond stress of $1.75\sqrt{f_c'}$ (where f_c' is the concrete compressive strength in MPa) over $l_{a,\mathrm{min}}$. This average bond stress, which is comparable to that used by Lowes and Altoontash,[24] was established assuming a linear slip distribution along $l_{a,\mathrm{min}}$ and the local bond stress reaching a maximum value of $2.5\sqrt{f_c'(\mathrm{MPa})}$ at the loaded end.[7] Accordingly,

$$l_{a,min} = \frac{f_y \pi d_b^{\,2}/4}{1.75\sqrt{f_c'}\pi d_b} = \frac{1}{7}\frac{f_y}{\sqrt{f_c'}}d_b, \tag{2}$$

where d_b is the bar diameter (mm).

Given the different values for variables d_b, f_y, and f_c' in the tests summarized in Table 1 and the dependency of the yield slip on these variables, Eq. (3) was established from a linear regression analysis as represented in Fig. 5 to determine the suitable value for s_y.

$$\mathrm{s_y(mm)} = 0.4\left(\frac{\mathrm{d_b(mm)}}{4}\frac{\mathrm{f_y(MPa)}}{\sqrt{\mathrm{f_c'(MPa)}}}(2\alpha+1)\right)^{1/\alpha} + 0.34, \tag{3}$$

where α is the parameter used in the local bond-slip relation as illustrated in Fig. 2 and was taken as 0.4 in this study in accordance with CEB-FIP Model Code 90 (MC90).[34]

As observed for the yield slip, it is conceivable that the loaded-end slip at the bar ultimate strength (s_u) and the stiffness reduction factor (b) are also functions of steel and concrete properties as well as the bar diameter. However, sufficient experimental data were not available to establish these functions from regression analyses; most of the tests summarized in Table 1 were terminated soon after reaching the yield slip. The limited test information available in the literature indicated that $s_u = 30 \sim 40 s_y$ and $b = 0.3 \sim 0.5$ would be appropriate. Furthermore, in the absence of sufficient experimental data, it is suggested that Eqs. (1) and (3) be used for sufficiently anchored bars with both straight and hooked ends under tension and compression loads. This suggestion should not introduce any significant error in the simulation of flexural members subjected to low axial loads (e.g., bridge columns and concrete walls in low- and mid-rise buildings). As more data become available, appropriate empirical equations suitable for defining s_u and b can be developed.

The applicability of Eq. (1) to describe the bar stress vs. loaded-end slip response under monotonic loading is demonstrated in Fig. 6 by comparing experimental data from two bar pull-out tests with the corresponding theoretical curves. The parameters used to define the theoretical curves are included in the figure, where the yield slips (s_y) were obtained using Eq. (3). The ultimate slip (s_u) reported in Fig. 6a was a measured value while s_u included in Fig. 6b was an estimated value based on the above recommendation. The b values were chosen in recognition of the observed initial slope of the hardening portion of the curves. A good agreement is seen between the theoretical curves and experimental data, indicating that Eq. (1) is capable of capturing the strain penetration effects in the analytical simulation of concrete flexural members.

Hysteretic Rules

To employ the proposed model for capturing the strain penetration effects in flexural members subjected to reversed cyclic loading, suitable hysteretic rules must be established for the bar stress vs. slip relationship. Using the experimental data reported by Lin[3] on cyclic response of a few well-anchored bars and observed cyclic response of columns reported in the next section, the following rules were established (see Fig. 7 for a graphical description):

- Prior to unloading, the maximum and minimum bar stresses and the corresponding slips are compared with the history values, and the variables (*maxrs*, *maxrl*) and (*minrs*, *minrl*) as indicated in Fig. 7 are updated if necessary.
- Unloading and reloading in any direction follows the linear elastic portion of the monotonic curve if the bar slip prior to unloading has never exceeded $+s_y$ or $-s_y$.
- When the bar slip has exceeded $+s_y$ or $-s_y$, the unloading in any direction follows a straight line with the elastic slope K until the bar stress reaches zero. The intersection between the straight unloading line and the s-axis is located as (*rsvg*, 0).
- A reloading path as defined by Eq. (4) is followed from the intersection point (*rsvg*, 0).

$$\sigma = \sigma^* \, maxrl \text{ or } \sigma = \sigma^* \, minrl \tag{4a}$$

$$\sigma^* = \frac{\dfrac{s^*}{s_{uy} - s^*}}{\left[\left(\dfrac{1}{s_{uy}}\right)^{R_c} + \left(\dfrac{s^*}{s_{uy} - s^*}\right)^{R_c}\right]^{1/R_c}}, \tag{4b}$$

$$s^* = \frac{s - rsvg}{s'_y} \tag{4c}$$

$$s_{uy} = \frac{maxrl - rsvg}{s'_y} \text{ or } \frac{minrl - rsvg}{s'_y} \tag{4d}$$

where σ^* is the bar stress ratio, s^* is the slip ratio, s_{uy} is the stress limit ratio, and s'_y is the elastic recovered slip determined by the return stress divided by the initial slope (K) as illustrated in Fig. 7.

- In Eq. (4), coefficient R_c, with typical values in the range of 0.5 to 1.0, defines the shape of the reloading curve. Depending on the anchorage detail and the corresponding mechanism, it is possible for a bar with sufficient anchorage length to exhibit pinching hysteretic behavior in the bar stress vs. slip response, especially when it is anchored into a joint. The coefficient R_c will permit the pinching characteristic to be accounted for in the analytical simulation of the flexural member. The lower end value of R_c will represent significant pinching behavior while a value of 1.0 will produce no pinching effect as demonstrated in Fig. 8. A comprehensive test program is required to establish a procedure to determine the value of R_c. In the absence of test data, the R_c values chosen for the examples may be used in fiber-based analysis of similar structural problems.

Material Model for Concrete Fibers

Similar to the model proposed for the steel fibers, a material model describing the monotonic response and hysteretic rules is also required for the concrete fibers. The combination of using the zero-length section element and enforcing the plane section assumption at the end of the flexural member imposes high deformations to the extreme concrete fibers in the zero-length element. These deformations were found to translate to concrete compressive strains in the order of 0.15 for the test columns described in the following section. According to the confinement model of Mander et al.,[35] these strains are significantly greater than the strain capacity estimated for the core concrete section of the columns used in following section. However, such large concrete strains are deemed appropriate for the analyses within the zero-length section element because the concrete at the end of the flexural member would benefit from additional confinement provided by the adjoining member. Furthermore, the plane section assumption will be violated at the end section of the flexural member due to the penetration effects.

In light of the discussion presented above, the concrete fibers in the zero-length was assumed to follow the Kent-Scott-Park stress-strain model and the corresponding hysteretic rules available in OpenSees through the material model known as Concrete01. To accommodate the large deformations expected to the extreme concrete fibers in the zero-length element, a perfectly plastic behavior was assumed for concrete in Concrete01 once the strength reduces to 80% of the confined compressive strength. A parametric study involving the three test units described below indicated that the simulation results were not very sensitive to the compressive strain chosen to trigger the perfectly plastic behavior for concrete.

EXAMPLES OF APPLICATION

To demonstrate the applicability of the zero-length section element with the proposed material models and the corresponding improvements to the analysis results, cyclic responses of two concrete columns and a bridge tee-joint system were simulated using OpenSees (Ver. 1.5) and the results were compared with the experimental data. For all examples, the existing Concrete01 and Steel02 elements were used, respectively, to model the concrete and steel fibers. Steel02 does not include any ratcheting effects. Concrete01 assume zero tension capacity, thus the tension stiffening is ignored.

For all analytical simulations with the strain penetration effects, the model parameters were determined as follows: the yield slips were calculated as per Eq. (3) using the reported material properties; the ultimate bar strengths were taken as $1.5f_y$ as per Priestley et al.[22]; the ultimate slips were approximated to $35s_y$; the b factors were taken as 0.5; and the R_c factors were taken as

1.0 for the columns and 0.7 for the Tee-joint system. The reason for using two different R_c factors was that the longitudinal bars in the cantilever columns had ample anchorage length and 90° hooks at the end, whereas the column bars were terminated into the tee-joint with straight ends and an anchorage length of $22d_b$. The suitable R_c values were determined by comparing the cyclic analysis results with the measured force-displacement responses of the test units.

Short Rectangular Column

The first of the two cantilever columns studied was short rectangular column U6 that was designed and tested by Saatcioglu and Ozcebe.[23] The testing of this column was part of a study that evaluated the effects of confinement reinforcement specified in ACI 318-83 on the ductility capacity of short columns. As shown in the insert of Fig. 9(a), this column had a square cross section and a clear height of 1000 mm above the footing, and was modeled using five fiber-based beam-column elements. After subjecting the column to a constant axial load of 600 kN, the lateral-load cyclic testing was performed and the measured force-displacement response is shown in Fig. 9(a). The test included sufficient instrumentation to quantify the displacement components due to member flexure, member shear, and strain penetration effects.

Also included in Fig. 9(a) are the simulated cyclic responses of the column with and without the zero-length section element to account for the strain penetration effects. (The simulation with the strain penetration effects used the following model parameters: s_y = 0.56 mm, f_y = 437 MPa, b = 0.5, and R_c = 1.0.) Between the two analyses, the one which included the strain penetration effects closely simulated the measured response. Because the response of the test unit was influenced by shear deformation, which is not included in the beam-column elements available in OpenSees, the simulation with the strain penetration produced somewhat larger load resistance than the measured response for a given lateral displacement. The discrepancies between the measured and experimental results are even greater for the simulation that ignored the penetration effects. This particular analysis also markedly overestimated the elastic stiffness, yield strength, and the unloading stiffness of the test unit.

A further comparison between the analysis results and experimental results is presented in Fig. 9(b), which shows the lateral deflection along the column height at the yield lateral displacement (Δ_y) and $4\Delta_y$. In this figure, the measured displacements reflect the flexural displacements including the strain penetration effects, which were established by subtracting the measured shear displacements (approximately 20% at Δ_y and 10% at $4\Delta_y$) from the measured column total displacements. The analytical displacements corresponded to the measured lateral loads of 310 kN at Δ_y and 350 kN at $4\Delta_y$, and the contribution of the strain penetration effects to the column flexural deformation measured at the top was about 50% at Δ_y and 30% at $4\Delta_y$, respectively. For both cases, the analysis simulation that included the strain penetration effects very closely captured the measured flexural displacements along the height of the column. The simulated column displacements without the strain penetration effects were significantly low.

Tall Circular Column

The second column investigated in this study was that tested by Smith[36], which served as the reference column for an investigation on strategic relocation of plastic hinges in bridge columns. This column had a circular section as shown in the insert of Fig. 10(a) and a clear height of 3658 mm above the column footing. Under constant axial load of 1780 kN, the yield displacement of the column was reported to be 40 mm and the corresponding lateral load resistance was 259 kN. The failure of the column occurred due to fracture of the longitudinal reinforcing bars at the column base, after attaining lateral displacement of 323 mm with lateral resistance of 356 kN.

Figure 10(a) compares the measured column top lateral displacement versus lateral force resistance with the analysis results, which were obtained with and without the zero-length element to capture the strain penetration effects and by modeling the column using five fiber-based beam-column elements. The analysis with the zero-length section element (with model parameters of s_y = 0.56 mm, f_y = 455 MPa, b = 0.5, and R_c = 1.0) more closely captured the measured response. In the pull-direction of loading, this analysis accurately predicted the lateral force resistance at the yield and maximum lateral displacements. In the push-direction, the analysis appears to have somewhat overestimated the maximum force resistance due to the measured load resistance in this direction being slightly smaller than the pull direction. On the other hand, the analysis that ignored the strain penetration effects overestimated the ultimate lateral load resistance and greatly underestimated the column lateral deflection for a given lateral load. The influence of the strain penetration on the overall cyclic response of the column was not as pronounced as that seen in Figs. 9 and 10 because the strain penetration effects on the overall force-displacement response diminish with increasing column height.

The column end rotation due to strain penetration reduces stress in the column longitudinal bars as is evident in Fig. 10(b). At the column yield displacement, the analysis that included the strain penetration effects correctly captured the strain distribution along a longitudinal extreme bar. The corresponding analysis without the strain penetration effects overestimated the bar strains in the plastic hinge region by about 30 percent. The strain gages in the hinge regions gradually failed when the column was subjected to inelastic displacements. Using the available data obtained at a column lateral displacement of 63 mm, Fig. 10(b) shows comparisons between the measured stain data and the calculated strain profiles. Again the analysis with the zero-length section element produced strains that closely matched with the measured strains along the bar.

The analysis that ignored the strain penetration effects overestimated the bar strains by as much as 50%. The measured strains at the two locations are smaller than the predicted values by the analysis that included the strain penetration effects. This discrepancy is believed to be mainly due to the calculated force at $1.6\Delta_y$ being slightly higher than the measured force resistance. The fact that the calculated and experimental steel strains fell in the yield plateau region made the discrepancy to appear large. Sudden strain increments are obvious in the calculated strain values near 732 mm in Fig. 10b. This is because the strain values above and below the point (also a node in the analysis) are calculated at Gauss integration points that belong to two beam-column elements. The interpolation algorithm in OpenSees does not guarantee consistency of fiber strains of adjacent elements.

Bridge Tee-Joint System

A bridge tee-joint system (specimen IC1) tested in an inverted position by Sritharan et al.[37] was studied to verify the feasibility of the proposed model for analyzing a structural system. This specimen with a conventional reinforced concrete cap beam, as schematically shown in Fig. 11(a), evaluated a new design method suitable for bridge cap beam-to-column joints. The concrete strengths on the day of testing were reported to be 31 MPa for the column and 40 MPa for the cap beam and joint. Under constant axial load of 400 kN, the column was subjected to cyclic lateral loading at a height of 1829 mm above the column-to-cap beam interface. The yield lateral displacement for the tee-joint system was reported to be 17 mm with the corresponding lateral resistance of 250 kN. The test joint experienced strength deterioration at lateral displacement of 103 mm due to formation of large joint cracks and subsequent joint damage.

The simulation model included six fiber-based beam-column elements for the cap beam and four beam-column elements for the column. An additional fiber-based beam-column element with the elastic column section properties modeled the joint. The zero-length section element (with the model parameters of s_y = 0.51 mm, f_y = 448 MPa, b = 0.5, and R_c = 0.7) was located between this elastic element and the adjoining column element.

Figure 11(a) compares the measured force-displacement hysteresis response of the test unit with the analytical results obtained with and without the strain penetration effects. The analysis, which included the strain penetration effects, produced force-displacement response that closely matched with the measured response in both loading directions. The joint shear failure experienced by the test unit towards the end of testing was not accounted for in the analytical model, and hence the analysis slightly overestimated the force resistance at the maximum displacement. On the other hand, the analysis that did not include the strain penetration effects overestimated both the lateral load resistance and the unloading-reloading stiffness.

The advantages of incorporating the strain penetration effects in the analysis is more pronounced in Fig. 11(b), in which the column moment vs. curvature histories at the beam-to-column intersection are compared. The analysis that ignored the strain penetration effects overestimated the column end curvature by approximately 90% towards the end of the test, indicating that the bar slip due to strain penetration greatly affects the local response measures that are indicative of damage to the plastic hinge region. A significant improvement to the moment-curvature response prediction was obtained when the analysis included the strain penetration effects. However, the predicted moment-curvature hysteretic loops are noticeably broad along the reloading path prior to intersecting the curvature axis. This discrepancy is expected to be diminished when the values of the model parameters, especially s_u, b, and R_c, are refined. As previously discussed, an experimental investigation designed to quantify the bar stress vs. slip response as a function of anchorage detail, bar diameter and material properties will improve selection of parameters for the steel fibers in the zero-length section element. Nonetheless, the tee-joint analysis results were adequate to emphasize the merit of the zero-length element concept and the proposed constitutive models to capture the strain penetration effects in fiber-based analysis of flexural concrete members.

CONCLUSIONS

Well-designed flexural concrete members experience rotations at the fixed end(s) due to bond slip that occurs as a result of strain penetrating along fully anchored longitudinal bars into the adjoining concrete members. Focusing on column and wall longitudinal bars anchored in footings and bridge joints, an efficient method is proposed in this paper to model the bond slip rotation using a zero-length section element that can be employed in nonlinear fiber-based analysis of concrete structures. A constitutive model that expresses the bar stress vs. loaded-end slip response was developed for the steel fibers of the zero-length section element using suitable experimental data reported in the literature. The adequacy of the proposed monotonic response for the steel fibers was illustrated by comparing the theoretical and measured bar stress vs. loaded-end slip responses of two pull-out tests conducted on fully anchored bars in concrete. Because of the lack of cyclic test data in the literature, the hysteretic rules for the bar stress vs. loaded-end slip response were established using the available test data and observed responses of concrete members under cyclic loading.

Advantages of the proposed method to improve fiber-based analysis of concrete structures was demonstrated by simulating cyclic response of two concrete cantilever columns and a bridge tee-joint system. Simulated responses were compared with the observed responses at both global and local levels. The analyses that utilized the proposed method to model the strain penetration effects satisfactorily captured the deflections, force vs. displacement hysteresis responses, strains in the longitudinal reinforcing bar and section curvature of the test units. When the strain penetration effects were ignored, the force resistance at a given lateral displacement was overestimated, along with portraying larger hysteresis loops. Most importantly, the local response parameters such as the steel strain and section curvature, which indicate the extent of structural damage, were grossly overestimated.

Based on these observations, it was concluded that 1) the strain penetration effects should not be ignored in the analysis of concrete members, and 2) the zero-length section element incorporating the proposed constitutive model for the steel fibers can be used in nonlinear fiber-based analysis to accurately capture the strain penetration effects and thus the global and local responses of concrete flexural members. The proposed method is versatile in that it can be used for modeling concrete flexural members without limiting cross-sectional shapes or direction of the lateral load. In addition, the proposed constitutive model for the bar stress vs. slip response can be employed to capture the strain penetration effects in models of concrete structures developed using other types of elements.

ACKNOWLEDGMENTS

The study reported in this paper is from a project supported by the National Science Foundation (NSF) under Grant No. CMS-0324559. The authors gratefully acknowledge the support of Drs. Steven McCabe and Doug Foutch, who have served as program directors for this grant. The authors also thank the collaborators of this project, especially Professor Cathy French, Suzanne Nakaki and Professor Ricardo López for their feedback on the proposed method for capturing the strain penetration effects. Any opinions, findings, and conclusions or recommendations expressed in this material are those of the authors and do not necessarily reflect the views of NSF.

NOTATION

b = stiffness reduction factor

d_b = bar diameter

f_c' = concrete compressive strength

f_y = bar yield strength

f_u = bar ultimate strength

K = initial slope of bar stress vs. loaded-end slip relation

l_a = anchorage length

$l_{a,\min}$ = the minimum anchorage length

R_c = power index of the unloading/reloading curve

R_e = power index of the envelope curve

s = loaded-end slip

$\tilde{s}$ = normalized loaded-end slip

s^* = slip ratio

s_1 = slip corresponding to the peak local bond stress

s_u = loaded-end slip when bar stress equals to the bar ultimate strength

s_{uy} = stress limit ratio

s_y = loaded-end slip when bar stress equals to the bar yield strength

s'_y = elastic recorvered slip

α = power index of the local bond-slip relation

$\bar{\varepsilon}$ = axial strain of a section

ε = fiber strain

φ = section curvature

μ = ductility coefficient

τ = local bond stress

τ_1 = peak local bond stress

σ = bar stress

$\tilde{\sigma}$ = normalized bar stress

σ^* = bar stress ratio

REFERENCES

1. Sritharan, S., Priestley, N., and Seible, F. "Nonlinear Finite Element Analyses of Concrete Bridge Joint Systems Subjected to Seismic Actions," *Finite Elements in Analysis and Design*. V. 36, 2000, pp. 215-233.
2. Sritharan, S., Vander Werff, J., Abendroth, R. E., Wassef, W., and Greimann, L., "Seismic Performance of a Concrete/Steel Integral Bridge Pier System," ASCE *Journal of Structural Engineering*, V. 131, No. 7, 2005, pp. 1083–1094.
3. Lin, I., "Anchorage characteristics for reinforcing bars subjected to reversed cyclic loading," Doctoral Dissertation, University of Washington, Seattle, WA, 1981, 326 pp.
4. Kowalsky, M., Priestley, N., and Seible, F., "Shear and Flexural Behavior of Lightweight iConcrete Bridge Columns in Seismic Regions," *ACI Structural Journal*, V. 96, No. 1, Jan.-Feb. 1999, pp. 136-148.
5. Calderone, A., Lehman, D., and Moehle, J., "Behavior of Reinforced Concrete Bridge Columns having Varying Aspect Ratios and Varying Lengths of Confinement," Report No. PEER 2000-08, 2000, University of California, Berkeley, CA.
6. Saatcioglu, M., Alsiwat, J. and Ozcebe, G. "Hysteretic Behavior of Anchorage Slip in R/C Members," ASCE *Journal of Structural Engineering*, V. 118, No. 9, 1992, pp. 2439-2458.
7. Eligehausen R., Popov E., and Bertero V. "Local Bond Stress-slip Relationships of Deformed Bars under Generalized Excitations," Report No. UCB/EERC 83-23, 1983, University of California, Berkeley.
8. Hawkins, N., Lin, I., and Ueda, T. "Anchorage of reinforcing bars for seismic forces." *ACI Structural Journal*, V. 84, No. 5, Sept.-Oct. 1987, pp. 407-418.
9. Popov, E. "Bond and Anchorage of Reinforcing Bars under Cyclic Loading," *ACI Journal*, V.

81, No. 4, July-August 1984, pp. 340-349.

10. Shima, H., Chou, L., and Okamura, H., "Bond-slip-strain Relationship of Deformed Bars Embedded in Massive Concrete," *Concrete Library of JSCE*, N0. 10, Dec. 1987, pp 79-94.
11. Malvar, L., "Bond of Reinforcement under Controlled Confinement." *ACI Material Journal*, V. 89, No. 6, Nov.-Dec. 1992, pp. 593-601.
12. Gilard, C. and Bastien, J., "Finite-element Bond-slip Model for Concrete Columns under Cyclic Loads." ASCE *Journal of Structural Engineering*. V. 128, No. 12, 2002, pp. 1502-1510.
13. Salem, H and Maekawa, K., "Pre- and Post-yield Finite Element Method Simulation of Bond of Ribbed Reinforcing Bars." ASCE *Journal of Structural Engineering*. V. 130, No. 4, 2004, pp. 671-680.
14. Lundgren, K. "Three-dimensional Modeling of Bond in Reinforced Concrete," Ph.D. Thesis, 1999, Chalmers University of Technology, Göteborg, Sweden. 143 pp.
15. Lowes, L. "Finite Element Modeling of Reinforced Concrete Beam-Column Bridge Connections," Doctoral Dissertation, 1999, University of California, Berkeley.
16. Filippou, F., Popov, E., and Bertero, V. "Effect of Bond Deterioration on Hysteretic Behavior of Concrete Joints." Report No. UCB/EERC 83-19, 1983, University of California, Berkeley.
17. Monti, G. and Spacone, E. "Reinforced Concrete Fiber Beam Element with Bond-slip." ASCE *Journal of Structural Engineering*. V. 126, No. 6, 2000, pp. 654-661.
18. Spacone, E., Filippou, F., and Taucer, F., "Fiber Beam-column Model for Nonlinear Analysis of R/C frames. Part I: Formulation," *Earthquake Engineering and Structural Dynamics*, V. 25, 1996, pp. 711–725.
19. Spacone, E., Filippou, F., and Taucer, F. "Fiber Beam-column Model for Nonlinear Analysis

of R/C frames. Part II: Applications," *Earthquake Engineering and Structural Dynamics*, V. 25, 1996, pp. 727–742.

20. Mayer, U. and Eligehausen, R. "Bond Behavior of Ribbed Bars at Inelastic Steel Strains," *2nd International Ph.D. Symposium in Civil Engineering,* 1998, Budapest.
21. Otani, S. "Inelastic Analysis of R/C Frame Structures," *Journal of the Structural Division*, Vol. 100, No. ST7, July, 1974, pp. 1433-1449.
22. Priestley, N., Seible, F., and Calvi, G., *Seismic Design and Retrofit of Bridges*, Wiley-Interscience. Hoboken, NJ 07030. 1996, 704 pp.
23. Saatcioglu, M. and Ozcebe, G. "Response of Reinforced Concrete Columns to Simulated Seismic Loading," *ACI Structural Journal*, V. 86, No. 6, Nov.-Dec. 1989, pp. 3-12.
24. Lowes, L. and Altoontash, A. "Modeling Reinforced Concrete Beam-column Joints Subjected to Cyclic Loading," ASCE *Journal of Structural Engineering*, V. 129, No. 12, 2003, pp. 1686-1697.
25. Ciampi V., Eligehausen R., Bertero V., and Popov E., "Analytical Model for Concrete Anchorages of Reinforcing Bars under Generalized Excitations," Report No. UCB/EERC 82-83, University of California, Berkeley, 1982.
26. Sritharan, S. "Analysis of Concrete Bridge Joints Subjected to Seismic Actions," Doctoral Dissertation, University of California, San Diego, California, 1998, 407 pp.
27. Mazzoni S., McKenna F., Fenves G. L., “Open System for Earthquake Engineering Simulation (OpenSees) User Manual, Pacific Earthquake Engineering Research Center, University of California, Berkeley, Ver. 1.5, 2004.
28. Building Code Requirements for Structural Concrete (ACI 318-02), American Concrete Institute, Farmington Hills, MI. 2002.

29. Maekawa, K., Pimanmas, A., and Okamura, H., *Nonlinear Mechanics of Reinforced Concrete*. 2003. Spon Press, 29 west 35th street, New York, NY 10001. pp. 392-398.

30. Shima, H., Chou, L., and Okamura, H., "Bond Characteristic in Post-yield Range of Deformed Bars," *Concrete Library of JSCE*, No. 10, Dec. 1987, pp. 113-124.

31. Mathey, R. and Watstein, D., "Investigation of Bond in Beam and Pull-out Specimens with High-yield-strength Deformed Bars," *Journal of the American Concrete Institute*, V. 32, No. 9, Mar. 1961, pp. 1071-1090.

32. Ueda, T., Lin, I., and Hawkins, N. "Beam Bar Anchorage in Exterior Column-Beam Connections," *ACI Structural Journal*, V. 83, No. 3, May-June 1986, pp. 412-422.

33. Viwathanatepa, S., Popov, E., and Bertero, V., "Effects of Generalized Loadings on Bond of Reinforcing Bars Embedded in Confined Concrete Blocks," Report No. EERC-79-22, University of California, Berkeley, CA., 1979.

34. FIB, Bulletin 10, "Bond of Reinforcement in Concrete", State of the art report prepared by Task Group Bond Models, former CEB, Task Group 5.2. fib, Case Postale 88, CH-1015 Lausanne , August 2000, 427 pp.

35. Mander, J., Priestley, M., and Park, R. "Observed Stress-strain Behavior of Confined Concrete," ASCE *Journal of Structural Engineering*, V. 112, No. 8, 1988, pp.1827-1849.

36. Smith, P. E., "Strategic Relocation of Plastic Hinges in Bridge Columns," MS Thesis, University of California, San Diego, California, 1996, 137 pp.

37. Sritharan, S., Priestley, N, and Seible, F., "Seismic response of column/cap beam tee connections with cap beam prestressing," Report No. SSRP-96/09, University of California, San Diego, California, 1996, 295 pp.

TABLES AND FIGURES

List of Tables:

List of Figures:

Table 1–Results of pull-out tests of deformed steel reinforcing bars

ID	f_c' (MPa)	d_b (mm)	l_a (mm)	f_y (Mpa)	s_y (mm)	$l_{a,\text{ min}}$ (mm)	Reference
1	37.6	10.2	673.1	403.3	0.3	95.5	Maekawa et al.[29]
2	19.6	19.1	762.0	350.3	0.5	215.4	Shima et al.[30]
3	19.6	19.1	762.0	610.2	0.9	375.3	
4	19.6	19.1	762.0	819.8	1.6	504.2	
5	28.6	12.7	266.7	708.8	0.5	240.4	Mathey et al.[31]
6	28.6	12.7	266.7	708.8	0.5	240.4	
7	26.1	12.7	355.6	708.8	0.8	251.6	
8	26.1	12.7	355.6	708.8	0.7	251.6	
9	32.1	12.7	431.8	708.8	0.6	227.1	
10	32.1	12.7	431.8	708.8	0.5	227.1	
11	27.7	25.4	711.2	537.8	1.0	370.7	
12	27.7	25.4	711.2	537.8	1.0	370.7	
13	28.0	25.4	863.6	537.8	0.8	368.8	
14	28.0	25.4	863.6	537.8	0.8	368.8	
15	28.8	19.1	609.6	438.5	0.4	222.6	Ueda et al.[32]
16	32.5	25.4	635.0	468.8	0.7	298.2	Viwathanatepa et al.[33]

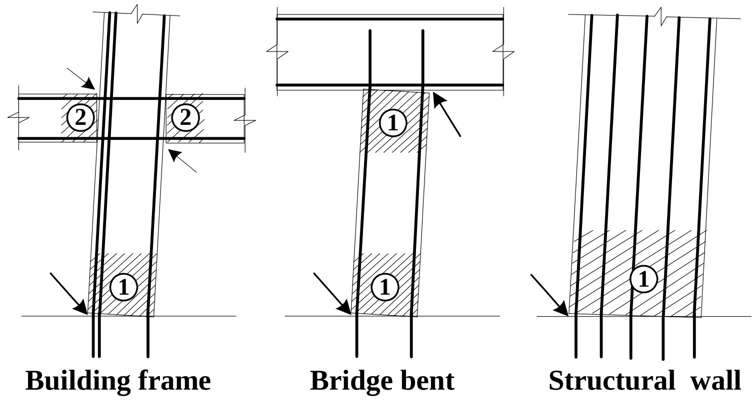

Fig. 1–Schematic representation of typical inelastic regions in well-designed concrete structures

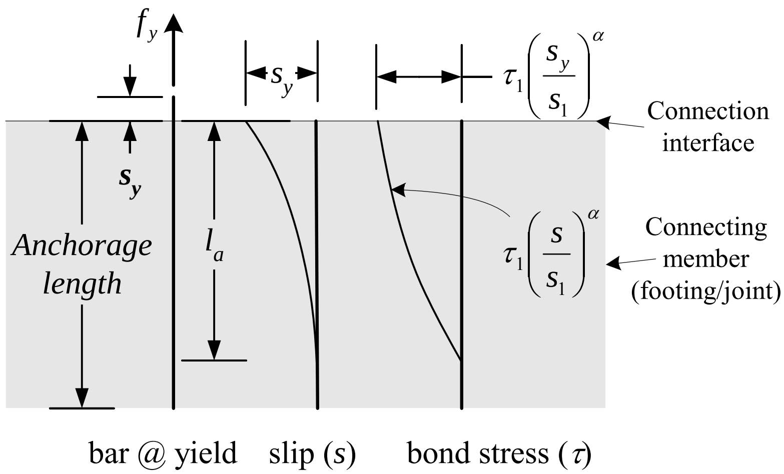

Fig. 2–Bond-slip due to strain penetration of a fully anchored bar at yield

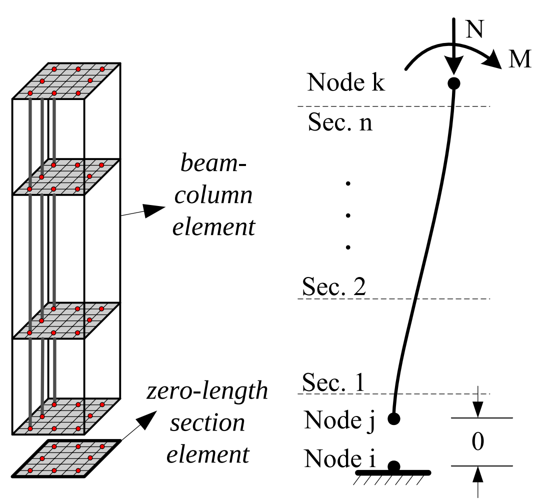

Fig. 3–Fiber-based modelling of strain penetration effects

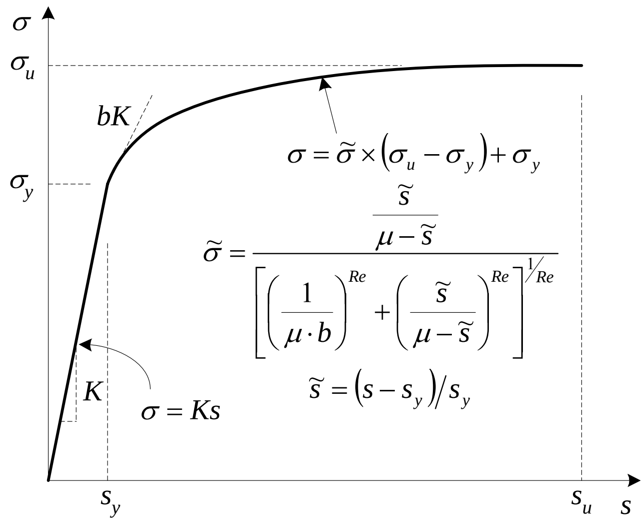

Fig. 4–Envelope curve for the bar stress vs. loaded-end slip relationship

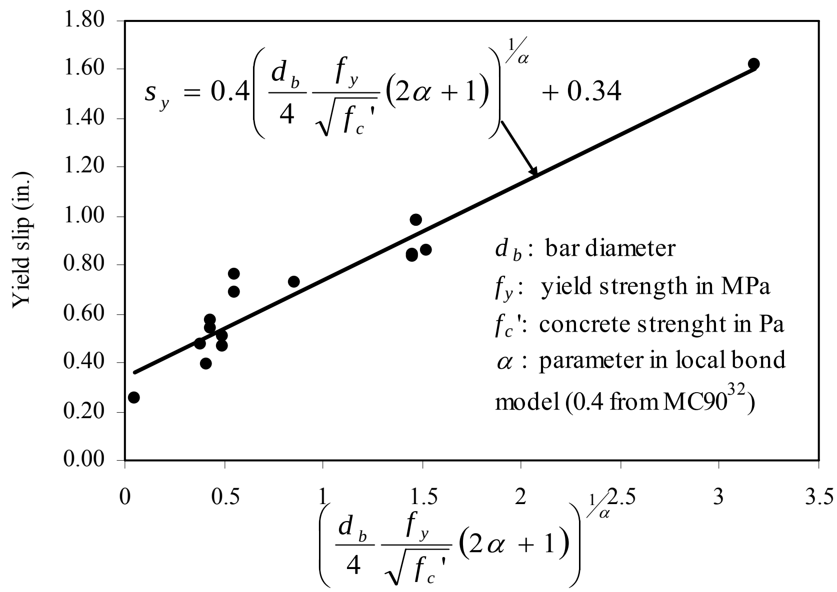

Fig. 5–Determination of bar slip at the yield strength

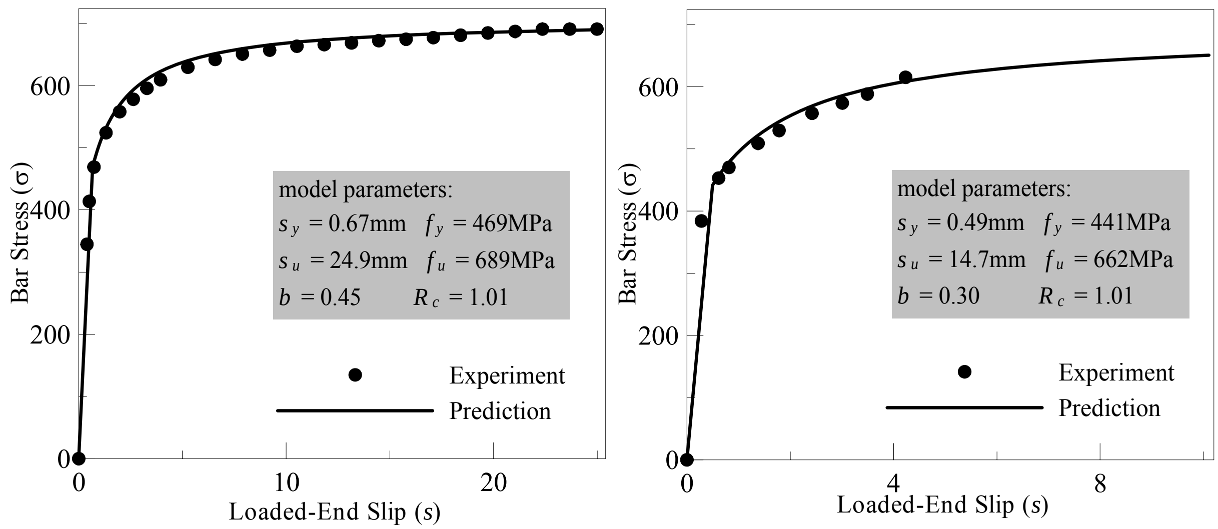

(a) Specimen #3 in Viwathanatepa et al.[31] (b) Specimen S64 in Ueda et al.[30]

Fig. 6–Experimental and analytical response of bar stress vs. loaded-end slip

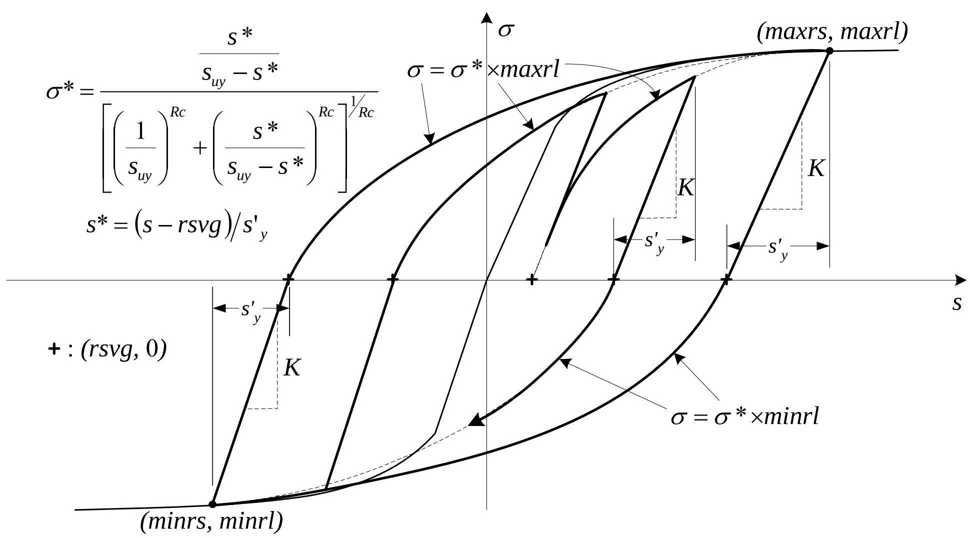

Fig. 7–Hysteretic model for the bar stress vs. loaded-end slip relationship

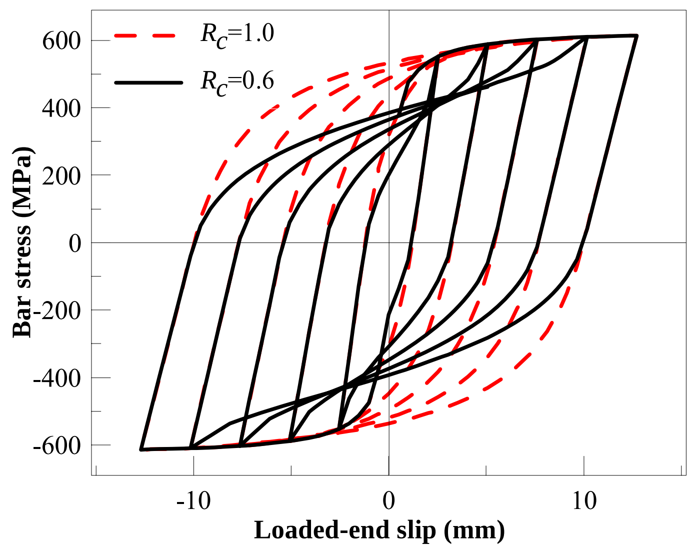

Fig. 8–The influence of parameter R_c on the cyclic bar stress vs. slip relation

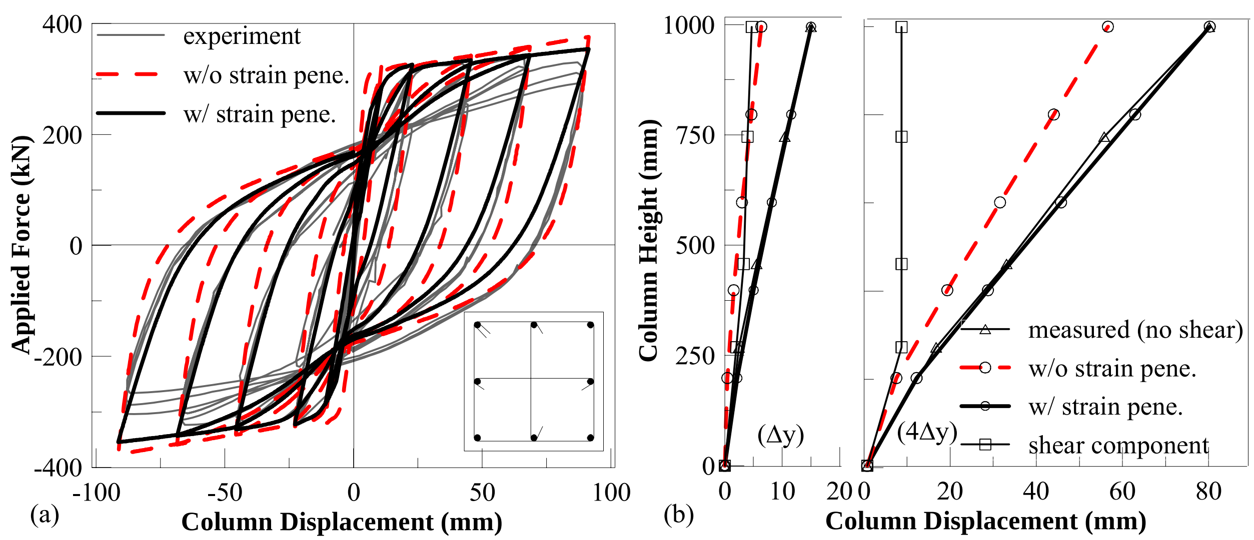

Fig. 9–Comparison of experimental and analytical results for short column specimen U6[21] (a) force vs. displacement; (b) deformation profile

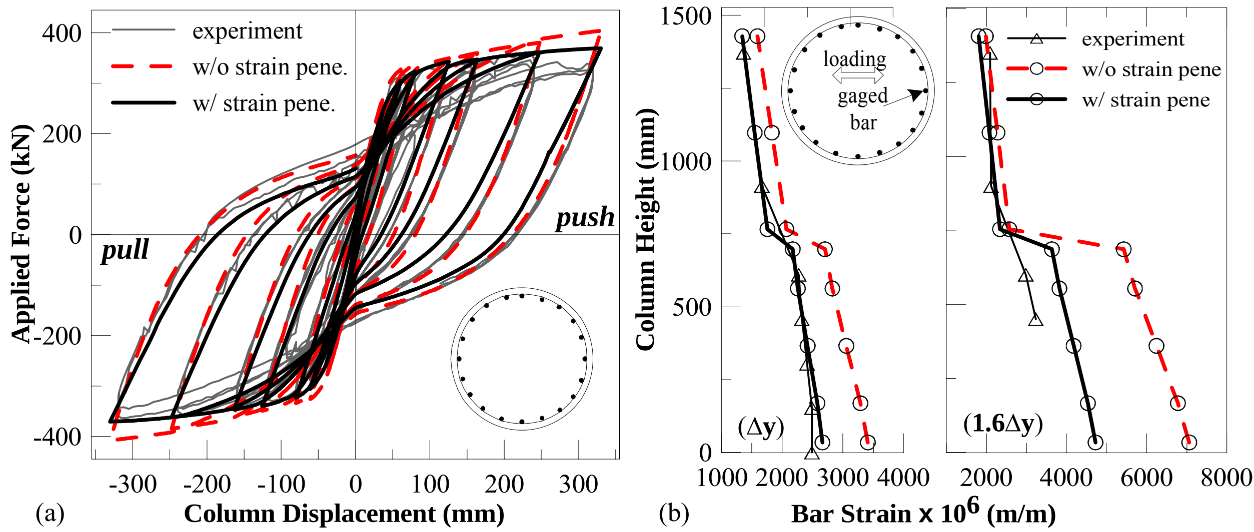

Fig. 10–Comparison of experimental and analytical results for a tall cantilever column[34]
(a) force vs. displacement; (b) strain distribution of an extreme bar

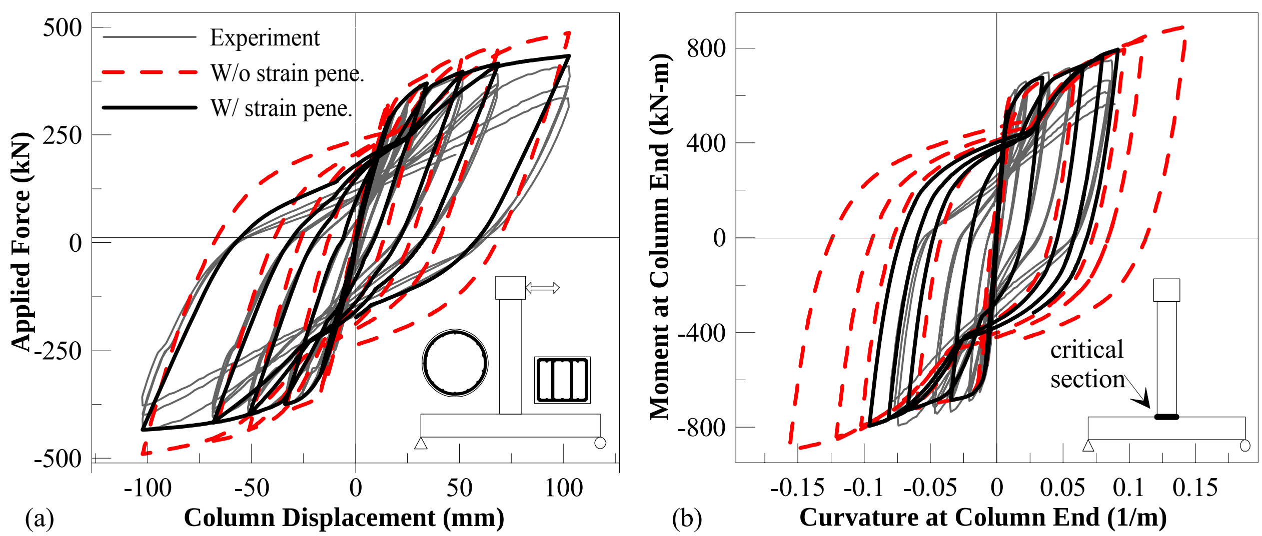

Fig. 11–Comparison of experimental and analytical results for T-joint specimen IC1[35]
(a) force vs. displacement; (b) moment vs. column end curvature